

Plasma Induced Variation of Electron Capture and Bound-State β Decays

B. Mishra^{1,2,*}, A. Pidotella¹, S. Taioli^{3,4}, S. Simonucci^{5,6} and D. Mascali¹

July 3, 2024

¹Istituto Nazionale di Fisica Nucleare - Laboratori Nazionali del Sud, Catania, Italy

²Dipartimento di Fisica e Astronomia - Università degli studi di Catania, Catania, Italy

³European Centre for Theoretical Studies in Nuclear Physics and Related Areas (ECT*), Bruno Kessler Foundation, Trento, Italy

⁴Trento Institute for Fundamental Physics and Applications (INFN-TIFPA), Trento, Italy

⁵School of Science and Technology, University of Camerino, Camerino, Italy

⁶Istituto Nazionale di Fisica Nucleare - Sezione di Perugia, Perugia, Italy

Abstract

The slow neutron capture (*s*-process) synthesises $\sim 50\%$ of all elements in the universe heavier than iron, whose abundances are determined by the competition between neutron capture and nuclear β -decay rates. The latter are expected to vary inside hot and dense plasmas such as those found in *s*-process nucleosynthesis sites. Here, we present a new and general theoretical study of the effect of local and non-local thermodynamic equilibrium ((N)LTE) plasmas on β -decays, using orbital electron capture (EC) decays in ${}^7\text{Be}$ as a model case. We begin from the model of Takahashi and Yokoi to calculate the lepton phase volume of ${}^7\text{Be}$ as a function of its ionisation state and excitation level, and consequently, the configuration-dependent EC decay rate. We then calculate the in-plasma ion charge state distribution (CSD) and level population distribution (LPD) for a grid of plasma density and temperatures, using the population kinetics code FLYCHK. By combining the configuration-dependent EC rate with the CSD and LPD, we calculate the in-plasma orbital EC rate in ${}^7\text{Be}$. The results show a strong correlation between the half-life and thermodynamic conditions of the plasma, underlining the importance of measuring decay rates in laboratory plasmas and the relevance of high precision atomic configuration models. The model discussed in this work is capable of calculating EC and bound state β decay (BSBD) rates in both low-density NLTE and high-density LTE plasmas.

We conclude by validating our model with state-of-the-art data in literature on isotopes of Pr and Dy, and by proposing future extension of the model to laboratory magnetoplasmas and stellar interiors aimed at improving nucleosynthesis models.

Introduction

Understanding the cosmic origin of elements has been a fascinating topic of study for decades. Since the seminal publications by Burbidge, Burbidge, Fowler and Hoyle [1] and Cameron [2], the field of nuclear astrophysics has made great strides in identifying the various processes constituting nucleosynthesis, and in quantifying the abundance of the elements. Among these reactions, the s -process occurs in asymptotic giant branch (AGB) and massive stars, synthesising $\sim 50\%$ of all elements between the iron peak and ^{208}Pb . The neutron density in these astrophysical sites $N_n \sim 10^6 \text{ cm}^{-3}$, leading to neutron captures on the same time scale as β -decays (days to few years). Consequently, the nucleosynthesis pathway proceeds along the valley of β -stability on the nuclear chart [3]. Stellar nucleosynthesis models developed for calculating s -process branching of heavy nuclei are thus sensitive to both neutron capture cross sections $\sigma(n, \gamma)$ and nuclear β -decay rates λ [4]. Uncertainties in either quantity can strongly affect the balance between the competing processes, leading to mismatch in observed and predicted elemental abundances [5, 6]. While there are experimental facilities already operational for measuring and/or updating relevant $\sigma(n, \gamma)$ to high precision [7, 8, 9], nucleosynthesis models still rely on decay half-lives $t_{1/2}$ measured in neutral atoms which may be significantly different from their stellar plasma counterparts.

Modification of λ due to changes in the atomic environment of radioactive nuclei has been investigated for decades [10]. The first studies on the subject involved measuring the rates in extreme physical environments, such as inside steel-encased cordite bombs [11] or at temperatures of liquid hydrogen [12]. However, only negligible changes ($< 0.05\%$) were observed. Further research found relatively larger changes on modifying the chemistry of the material containing the decaying nuclei, such as using a fluoride or oxide of the isotope instead of the metal [13, 14], or implanting the nucleus into different compounds [15, 16, 17]. This effect was attributed to perturbation of the electron density on the nuclear surface which affected electron capture rates, in line with the the hypotheses of Daudel and Segre [18, 19]. The same phenomenon was also observed in internal conversion rates of isomers such as ^{99m}Tc and ^{90m}Nb [20, 21].

A much stronger effect of the atomic environment on λ was observed in highly charged ions (HCIs) circulating in storage rings. The first such experiment was performed by Jung, Bosch and coworkers [22] who investigated the decay of fully-stripped $^{163}\text{Dy}^{66+}$ ions. They discovered that the isotope became suddenly unstable (neutral ^{163}Dy is stable) and rapidly transmuted into ^{163}Ho through bound state β decay (BSBD), making it the first observation of this

phenomenon. Soon after, Bosch, Faestermann and coworkers discovered BSBD in fully-stripped ^{187}Re [23] and measured a dramatic reduction in $t_{1/2}$ from 42 Gyr in neutral ^{187}Re to 32.9 ± 2 yr in $^{187}\text{Re}^{75+}$. Since the $^{187}\text{Re}/^{187}\text{Os}$ pair is used as a cosmochronometer due to its long $t_{1/2}$, a nine order increase in λ meant re-evaluation of the galactic age based on its actual $t_{1/2}$ in the stellar interior. A recent review by Litvinov and Chen [24] lists all the HCIs whose $t_{1/2}$ has been measured in storage rings, and offers valuable insights into BSBD and electron captures (EC) in single-charge species. Various aspects of the phenomenon have been studied theoretically over the years, and consequently, several formulations have been developed to calculate changes in $t_{1/2}$ in different materials [25, 26, 27] and in fully-stripped ions [28, 29, 30].

The interior of stars where nucleosynthesis occurs is a naturally occurring dense plasma which contains isotopes in various ionisation stages surrounded by an energetic electron cloud. It can thus be expected that decay rates will vary strongly, depending on the properties of the plasma. Palmerini [5] and Busso [6] speculated on possible plasma-induced variation of decay rates in isotopes of Cs, Lu, Nb, Zr and Kr - among others - to quantify their impact on modelling the abundance of *s*-process elements. Their work was complemented by Taioli and Simonucci who developed *ab-initio* Dirac-Hartree-Fock (DHF) models to predict $t_{1/2}$ of ^{134}Cs and ^{135}Cs as a function of plasma temperature and density [31]. In addition to the aforementioned radio-isotopes, in-plasma decay rate of ^7Be has attracted a great deal of attention from researchers. Bahcall, Iben and Gruzinov worked extensively on EC decays in ^7Be [32, 33, 34, 35, 36, 37], analysing in detail their relative contribution compared to continuum capture rates in the interior of the sun. The topic witnessed a renewed interest in recent years, with new predictions about the $t_{1/2}$ of ^7Be calculated using updated *ab-initio* models and its impact on the solar neutrino production discussed [38, 39, 40, 41, 42]. Coincidentally, many of the experiments investigating chemically-induced changes in λ mentioned earlier also involved ^7Be , underlining the historical role played by this isotope in this field. Studying ^7Be is also important for the cosmological lithium problem, where the abundance of ^7Li is calculated from a series of interconnected reactions, one of which is $^7\text{Be}(e^-, \nu_e)^7\text{Li}$ [37, 42, 43].

The first comprehensive theories on β -decay in stellar plasma were proposed by Bahcall [44, 45, 46], and covered continuum decays and captures in great detail. A full theoretical analysis of all in-plasma β -decay processes was made by Takahashi and Yokoi [47] (hereafter TY83) who put forward elegant expressions for calculating the lepton phase volume associated with each decay channel and showed how the stellar plasma may cause enhancement/suppression of some transitions. Their formulations were also used to predict BSBD rates in fully-ionised nuclei by Gupta [28] and Chang [29] and their coworkers, reproducing the observations from storage rings [22] in the process.

In order to benchmark TY83 and study plasma-induced changes in β -decay rates experimentally, a new facility named PANDORA (Plasmas for Astrophysics, Nuclear Decay Observations and Radiation for Archaeometry) is under realisation at INFN-LNS in Catania, Italy [48]. The facility aims to use an electron cyclotron resonance ion source to trap a compact magnetoplasma that

can emulate certain aspects of the stellar interior like the presence of a charge state distribution (CSD) in ions and a cloud of energetic electrons forming a continuum. By injecting radioisotopes into the plasma and measuring decay rates as a function of density and temperature, it would be possible to estimate stellar $t_{1/2}$ with greater accuracy than through experiments in storage rings or electron beam ion traps [49, 50] that cannot reproduce plasma effects [51].

In its original formalism, the TY83 model predicts β -decay rates in spatially homogeneous plasmas under local thermodynamic equilibrium (LTE) wherein ion CSD, level population distribution (LPD), and electron properties are respectively defined by the Saha, Boltzmann and Maxwell distributions through a single unified temperature. In this work, to generalise TY83 for any kind of plasma - including low density non-LTE (NLTE) laboratory magnetoplasmas - we have split the model into two components:

- An *atomic component*, which calculates the decay rate of the radio-isotope as a function of its charge state i and excitation level j (hereafter referred to as the *configuration-dependent decay rate* $\lambda^*(ij)$)
- A *plasma component*, which calculates the CSD and LPD associated with the radio-isotope as a function of plasma density and temperature (hereafter denoted by the *probability factor* p_{ij})

The in-plasma decay rate can then be obtained by combining p_{ij} with $\lambda^*(ij)$. By disentangling the two components, it is possible to analyse the fundamental coupling of atomic and nuclear properties independent of the plasma, and then incorporate the effects of the latter through the p_{ij} factors.

Differently from LTE plasmas, p_{ij} in NLTE plasmas are obtained using population kinetics codes which generate a full reaction rate matrix coupling all charge states and excitation levels through a collision-radiative (CR) model, and iteratively solve it till plasma steady state is reached. In this work, we investigate the variation of β -decay rates in a generic plasma using the coupled atomic and plasma components. We discuss our approach through the example of orbital EC decay in ${}^7\text{Be}$, but the formalism is identical for BSBD as well. The choice of this isotope is motivated by its simple atomic nature which facilitates analysis, but it also has fundamental importance in several astrophysical models, such as in calculating the solar neutrino flux mentioned earlier.

Methods and Results

The methodology used to investigate the plasma effects on the β -decay rate consist of multiple steps: first, we calculate $\lambda^*(ij)$ following the technique outlined in TY83 and then use the population kinetics code FLYCHK [52] to calculate p_{ij} under different plasma conditions. We then calculate in-plasma orbital EC decay rates as a function of plasma electron density (n_e) and temperature (kT_e), in both low-density NLTE (corresponding to laboratory conditions) and high-density LTE systems (corresponding to stellar interiors). We benchmark our

results with independent, *ab-initio* calculations, as well as with experimental data. Finally, we conclude by highlighting the versatility of the model, and with perspectives on how to adapt it for the PANDORA facility.

Configuration-Dependent EC Decay Rate of ${}^7\text{Be}$

${}^7\text{Be}$ decays into ${}^7\text{Li}$ through the electron capture process



where the captured e^- may belong to either the continuum or an atomic orbital. In case of the former, the decay is classified as *continuum capture*, while the latter is termed as *orbital capture*. Under neutral conditions, the decay is spontaneous with Q -value $Q_0 = 861.815$ keV for the ground state $3/2^- \rightarrow 3/2^-$ and $Q_1 = Q_0 - 477.6 = 384.215$ keV for the excited $3/2^- \rightarrow 1/2^-$ transition. These values represent the difference between the atomic mass energies of the parent and daughter systems, and therefore already include a small contribution from the binding energy of the electrons. Both are allowed transitions, with the former being mixed Fermi and Gamow-Teller and the latter being pure Gamow-Teller. They are characterised by comparative half-lives $\log f_0 t = 3.324$ and $\log f_1 t = 3.556$, respectively [53]. The comparative half-lives are simply a product of the lepton phase volume f , and the half-life $t_{1/2}$, and depend only on the nuclear matrix element fixed by the levels of parent and daughter nuclei. The transitions are henceforth indexed by m for brevity, where $m = 0$ and $m = 1$ represent the decay to the ground and excited states of ${}^7\text{Li}$, respectively.

The lepton phase volume f describes the phase space accessible to the electron and neutrino during the decay. It varies with the atomic configuration (ij) of the radio-isotope ion and the type of transition m . According to the formulation of TY83, the configuration-dependent phase volumes $f_m^*(ij)$ of orbital EC and BSBD can both be calculated as

$$f_m^*(ij) = \sum_x \sigma_x \frac{\pi}{2} [g_x \text{ or } f_x]^2 (Q_m(ij)/m_e c^2)^2 S_{(m)x} \quad (2)$$

where x represents the atomic orbital from where the electron is captured (in case of EC) or into which it is emitted (in case of BSBD), $Q_m(ij)$ is the decay Q -value which varies with the ion configuration, $m_e c^2$ is the electron rest mass energy, $[g_x \text{ or } f_x]^2$ is the larger of electron radial wavefunction evaluated at the nuclear radius, and $S_{(m)x}$ is the shape factor. The quantity σ_x represents the occupancy of the orbital x .

The configuration-dependent EC decay rate in ${}^7\text{Be}$ can be calculated as

$$\lambda^*(ij) = \ln 2 \left(\frac{f_0^*(ij)}{f_0 t} + \frac{f_1^*(ij)}{f_1 t} \right) \quad (3)$$

where $f_0 t$, $f_1 t$ are the aforementioned ft values.

The configuration-dependent $Q_m(ij)$ can be evaluated as

$$Q_m(ij) = Q_m + [B_{\tau_{\text{Be}^i}}^* - B_{\tau_{\text{Li}^{i'}}}^*] + [e_{\tau_{\text{Be}^i, j}}^* - e_{\tau_{\text{Be}^{i'}, j'}}^*] \quad (4)$$

where $Q_m = Q_0$ or Q_1 , $B_{\tau_{Be^i}}^* - B_{\tau_{Li^{i'}}}^*$ is difference in electronic binding energies when the atoms are in the charge states i and i' respectively, and $e_{\tau_{Be^i,j}}^* - e_{\tau_{Li^{i'},j'}}^*$ is the difference in energy of excitation levels j and j' . The bracketed terms denote the contribution of atomic ionisation and excitation to the decay Q -value, and when $(i', j, j') \rightarrow 0$, $Q_m(i, j) \rightarrow Q_m$. This formalism is an extended version of the one used by Gupta and Chang [28, 29, 30], applicable to any ij -configuration, and not just fully-stripped atoms.

In its present form, Eq. 4 allows calculating the modification of Q_m due to a single coupling between parent configuration ij and daughter configuration $i'j'$. However, given a configuration ij of ${}^7\text{Be}$, any $i'j'$ -configuration of ${}^7\text{Li}$ may be synthesised, as long as the effective $Q_m(ij \rightarrow i'j') > 0$. Naturally, the ij -configuration should also have electrons in the relevant shell to allow capture. Consequently, $Q_m(i, j)$ should be calculated by fixing the configuration ij of ${}^7\text{Be}$ consistent with the type of capture, and coupling it with all configurations of ${}^7\text{Li}$ and then averaging the results. In this way, Eq. 4 can be re-written as

$$Q_m(i, j) = Q_m + \bar{\Delta}\epsilon^{ij} \quad (5)$$

where $\bar{\Delta}\epsilon^{ij}$ now represents the total modification in Q_m on account of the ij -configuration coupling. The term is calculated as

$$\bar{\Delta}\epsilon^{ij} = \epsilon_{\tau_{Be^i,j}}^* - \frac{1}{N} \sum_{i'j'} \epsilon_{\tau_{Li^{i'},j'}}^* \quad (6)$$

where the summation $\sum_{i'j'}$ is over all daughter configurations resulting in positive energy difference and N represents the total number of those levels. Here $\epsilon_{\tau_{Be^i,j}}^*$ and $\epsilon_{\tau_{Li^{i'},j'}}^*$ represent the total energy of their respective configurations, obtained by summing the ionisation potentials of all preceding charge states $i/i' = 0, 1, \dots, i - 1$ and the energy of level j/j' relative to the ground state. This formalism is equivalent to that of Eq. 4, with the exception that the binding energies are replaced by the ionisation potentials. For sake of simplicity, it is assumed that the decay does not result in a change in the charge state of ${}^7\text{Li}$ such that $i = i'$ and only bound levels within the same ionisation state are coupled (no internal conversion).

We use the atomic level descriptions in the population kinetics code FLYCHK [52] to generate a configuration-coupling scheme capable of calculating $\bar{\Delta}\epsilon^{ij}$ as a function of (ij) . A detailed description of the nomenclature, spectroscopic notation and electronic configuration of FLYCHK levels is provided in the Appendix. An example of the level coupling scheme and aforementioned averaging procedure is shown in Fig. 1 using K-shell capture in ${}^7\text{Be}^{0+}$ and L-shell capture in ${}^7\text{Be}^{1+}$. It can be seen that in some cases, only certain configurations of the parent nucleus can contribute to the capture - e.g., L-capture requires the presence of at least one electron in the L-shell and thus only the first two levels in ${}^7\text{Be}^{1+}$ can contribute to the decay.

Fig. 2 shows the variation in $Q_0(i, j)$ for various configurations of ${}^7\text{Be}$, which is basically the energy of the neutrino ν_e . The X-axes in the plots list a few level names, while the Y-axes show the difference between $Q_0(i, j)$ and Q_0 . Since

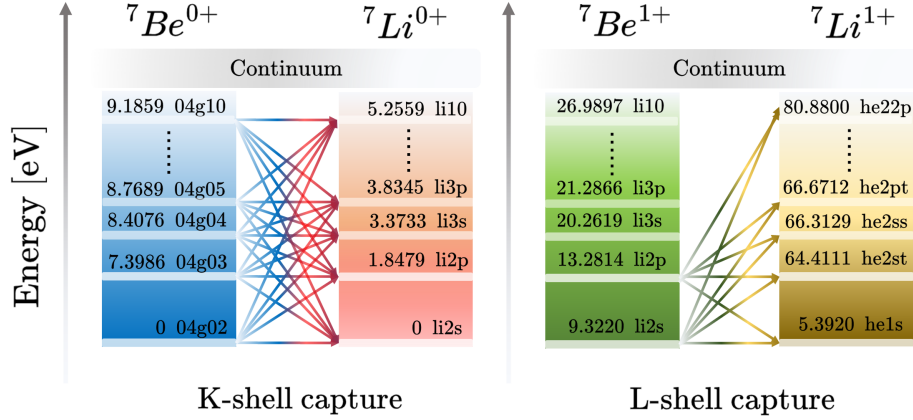
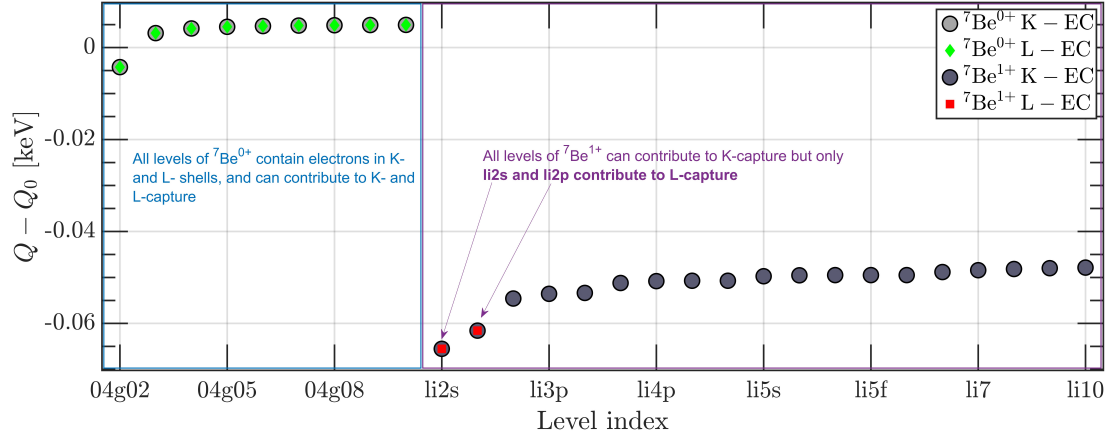


Figure 1: Atomic level coupling scheme to calculate $\bar{\Delta}\epsilon^{ij}$ for (a) K-shell and (b) L-shell capture. The continuum band represents all levels whose energy exceeds the ionisation potential, and are excluded from the coupling. The arrows indicate which levels of ${}^7\text{Be}^{i+}$ can contribute to the capture, and which levels of ${}^7\text{Li}^{i+}$ can be produced. The level energies are placed on the left of each coloured box, while the level index is placed on the right. Detailed information on the level notations can be found in the Appendix.

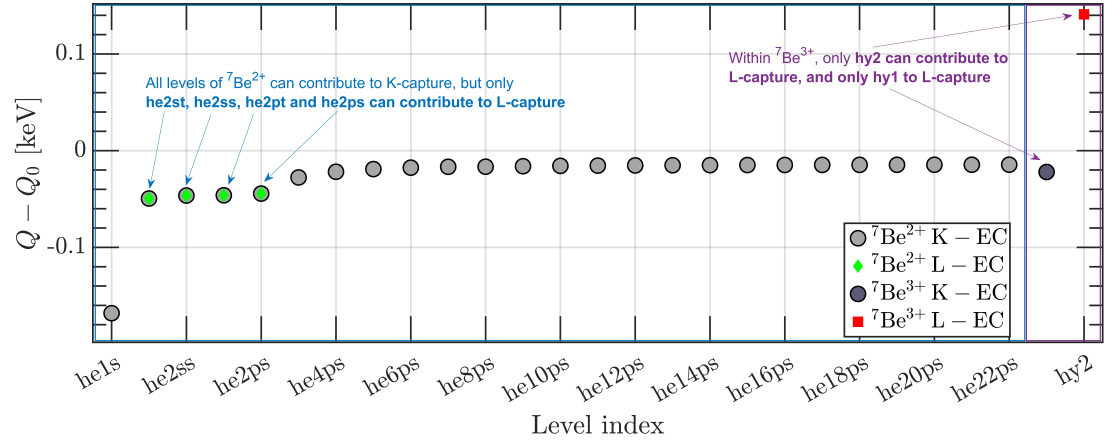
$Q_0 = 861.885$ keV, none of the configurations prohibit the decay because their Q -variations are on the eV scale, but there are fluctuations nonetheless. Deviations on the eV scale are anyway acceptable because the neutrino created in the decay process carries away the energy and balances the energetics of the reaction. The overlap between the K- and L-capture plots shows that in neutral ${}^7\text{Be}$, all levels participate in *both* K- and L-capture but only certain levels can do the same from $i = 1^+$ onward. These points are also detailed in the plots.

The shape factor $S_{(m)x}$ is defined by the type of transition and orbital from which the electron is captured [47]. For allowed transitions such as in ${}^7\text{Be}$, $S_{(m)x} = 1$ when capturing electrons from $x = 1s_{1/2}, 2s_{1/2}, 2p_{1/2}$ and $S_{(m)x} = 0$ for $x = 2p_{3/2}$. Electrons beyond the L-shell have low capture probability and are consequently neglected. The shape factors are born from the selection rules and conservation of spin-parity between nucleon and lepton wavefunctions and are consistent with the explanation provided by Folan and Tsifrinovich [56]. Here we use the spectroscopic notation $x = nl_{j=l+s}$ to denote the atomic orbitals.

The quantities f_x and g_x describe the overlap between the electronic orbital and the nuclear surface, assuming that the capture takes place within a thin, shell-like region at the nuclear boundary. In principle, the capture may take place inside the entire nucleus, but a rigorous analysis of the overlap between nucleons and electrons in the nuclear interior by Morresi and coworkers [57] produced no significant difference with respect to pure surface capture alone, and thus the assumption still holds. f_x and g_x are calculated through the



(a)



(b)

Figure 2: $Q_0(ij) - Q_0$ for different j in (a) ${}^7\text{Be}^{0,1+}$ and (b) ${}^7\text{Be}^{2+,3+}$. No plot is shown for fully-ionised ${}^7\text{Be}$ because it is void of electrons for capture. For sake of brevity, only a few levels in each ionisation stage are shown, but important levels are marked in the plots. $Q_m(ij)$ is basically the energy of the emitted neutrino.

expressions

$$f_x = f_\kappa(r)|_{r=R} = f_\kappa(R) \quad (7)$$

$$g_x = g_\kappa(r)|_{r=R} = g_\kappa(R) \quad (8)$$

where $f_\kappa(r)$, $g_\kappa(r)$ are radial wavefunctions associated with the orbital x , the parameter κ is related to the spin and angular momentum of the same orbital [58], and R is the phenomenological nuclear radius $R = R_0 A^{1/3}$ expressed in atomic units, with $R_0 = 1.2$ fm. The radial wavefunctions can be calculated as

$$f_\kappa(r) = \left(\frac{\hbar}{m_e c a_0} \right)^{3/2} \frac{P_\kappa(r)}{r} \quad (9)$$

$$g_\kappa(r) = \left(\frac{\hbar}{m_e c a_0} \right)^{3/2} \frac{Q_\kappa(r)}{r} \quad (10)$$

where a_0 is the Bohr radius and $P_\kappa(r)$, $Q_\kappa(r)$ are the eigenfunctions of the radial component of the Dirac equations in a central Coulomb field of potential V

$$\frac{dP_\kappa(r)}{dr} = -\frac{\kappa}{r} P_\kappa(r) - \left(2c' + \frac{V - \epsilon}{c'} \right) Q_\kappa(r) \quad (11)$$

$$\frac{dQ_\kappa(r)}{dr} = \frac{\kappa}{r} Q_\kappa(r) + \left(\frac{V - \epsilon}{c'} \right) P_\kappa(r) \quad (12)$$

where c' is the speed of light in atomic units and ϵ is the energy of the orbital. The coefficient $\hbar/m_e c a_0$ in Eqs. 9 and 10 converts $P_\kappa(r)$, $Q_\kappa(r)$ from atomic to natural units.

Being eigenfunctions of the radial component alone, $P_\kappa(r)$, $Q_\kappa(r)$ obey the normalisation condition

$$\int_0^\infty [P_\kappa(r)^2 + Q_\kappa(r)^2] dr = 1 \quad (13)$$

where $[P(r)^2 + Q(r)^2] dr$ represents the radial charge *probability*, i.e. the probability of finding an electron at a certain distance r from the nucleus. On the other hand, $f_\kappa(r)$ and $g_\kappa(r)$ obey the normalisation condition

$$\int_0^\infty [f_\kappa(r)^2 + g_\kappa(r)^2] r^2 dr = 1 \quad (14)$$

because $f_\kappa(r)^2 + g_\kappa(r)^2$ represents the charge *probability density*. This means that while certain orbitals may have non-zero probability density at the centre of the nucleus ($f_\kappa(r)^2 + g_\kappa(r)^2 \neq 0$ for $r \rightarrow 0$), the *probability* of electrons being there is zero because $[f_\kappa(r)^2 + g_\kappa(r)^2] r^2 \rightarrow 0$.

We use the analytical solutions to Eqs. 11 and 12 as derived in Ref [58] to calculate f_x and g_x . Fig. 3(a) shows the radial charge probability as a function of r for different orbitals in ${}^7\text{Be}$. The plots corresponding to $x = 2p_{1/2}$ and $2p_{3/2}$ overlap with each other on account of their similarity. It can be seen that

all orbitals have probability maxima, but in addition to this, the $x = 2s_{1/2}$ also has a probability minimum, which denotes the node of the wavefunction. The larger of f_κ^2 or g_κ^2 as a function of r is shown in Fig. 3(b). The dotted vertical line in the same plot denotes the nuclear surface, and the intersection of the two represents f_x^2 or g_x^2 . It can be easily seen that compared to $x = 1s_{1/2}$ and $x = 2s_{1/2}$, outer orbitals penetrate extremely weakly into the nucleus. K-captures are the strongest processes followed by L-captures which are almost entirely carried out by electrons in the $x = 2s_{1/2}$ orbitals.

The occupancy σ_x is a number between 0 and 1 which describes the completeness of an orbital, with the former meaning completely empty and the latter meaning completely full. It is calculated according to the usual Pauli exclusion principles for atomic shell filling. To use Eq. 2 identically for both EC and BSBD, σ_x can be generalised as

$$(\sigma_x)_{EC} = 1 - (\sigma_x)_{BSBD} \quad (15)$$

We calculate the occupancy of the K- and L-shell orbitals approximately using the level descriptions of FLYCHK whose spectroscopic notations are often a direct representation of electron distribution in various orbitals.

By combining all the above quantities with Eqs. 2 and 3, we obtain the configuration-dependent EC rate $\lambda^*(ij)$ in ${}^7\text{Be}$. To demonstrate the effect of the ionic configuration better, we calculate the percentage change in EC decay rate $\delta\lambda^*(ij)$ as

$$\delta\lambda^*(ij) = \frac{\lambda^*(ij) - \lambda(0)}{\lambda(0)} \times 100\% \quad (16)$$

where $\lambda(0)$ is the decay rate of neutral, ground state ${}^7\text{Be}$. The results are shown in Fig. 4.

It is evident that the ${}^7\text{Be}$ EC decay rate varies for all excitation levels, but the variation is strongest in doubly and triply-ionised states. For the neutral and $i = 1^+$ ionisation states, $\delta\lambda^*(ij)$ is driven by $Q(ij)$, as can be corroborated by Fig. 2. The small spike in capture rate at $\text{li}2s$ is a model-artifact, arising from the fact that $\sigma_{2s} = 0.5$ for this level, whereas the same for levels in neutral ${}^7\text{Be}$ is smaller and subject to greater uncertainty. This is due to the lack of precision in the electronic configuration of neutral atoms in FLYCHK data, as is described in more detail in the Appendix. The deviations are quite small, however, and may be neglected. For $i = 2^+$ and $i = 3^+$, the major factor is the occupancy of the K and L-shells. Since K-shell captures carry more weight compared to their L-shell counterparts, a rapid drop from $\sigma_{1s} = 100\%$ in $\text{he}1s$ to $\sigma_{1s} = 50\%$ in $\text{he}2st$ (Fig. 4(b)) results in an almost equal drop in decay rates. The rate decreases again going from $\text{he}2ss$ to $\text{he}2pt$ when L-captures switch from $2s$ to $2p_{1/2}$ orbitals. The final sharp drop by 50% in ${}^7\text{Be}3^+$ when going from $\text{hy}1$ to $\text{hy}2$ is explained by the excitation of the one attached electron from the K- to L-shell.

The $\lambda^*(ij)$ calculated here are validated against independent results from the relativistic Dirac-Hartree-Fock model [31, 41, 57] and the match between the two rates can also be appreciated in Fig. 5. The small mismatch at $\text{li}2s$ is

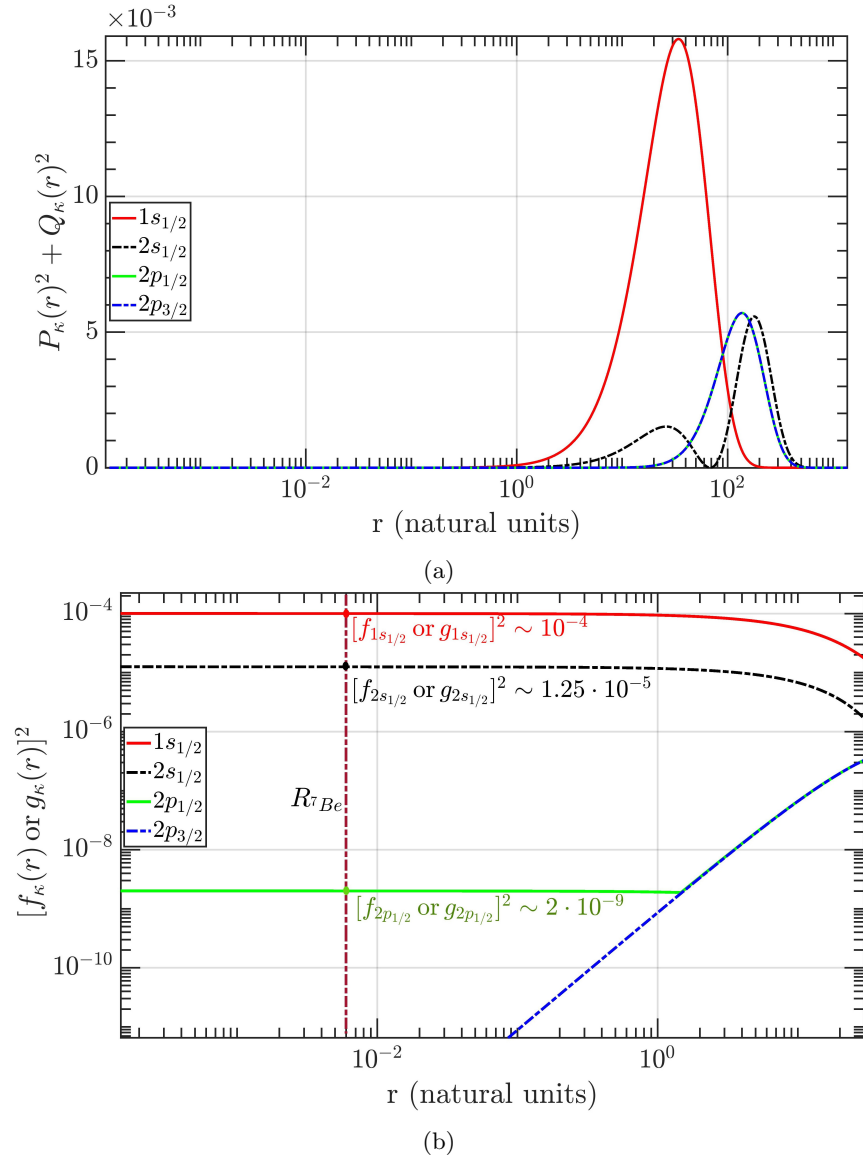
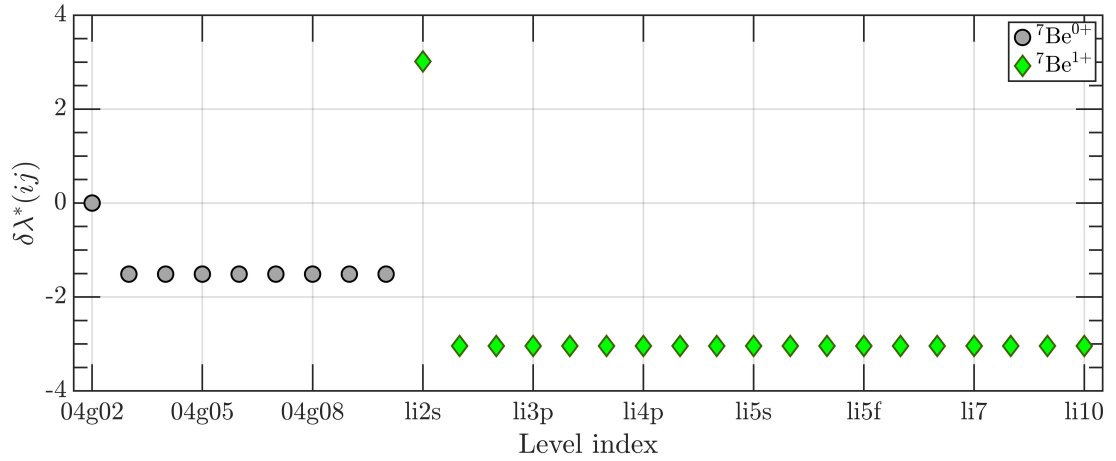
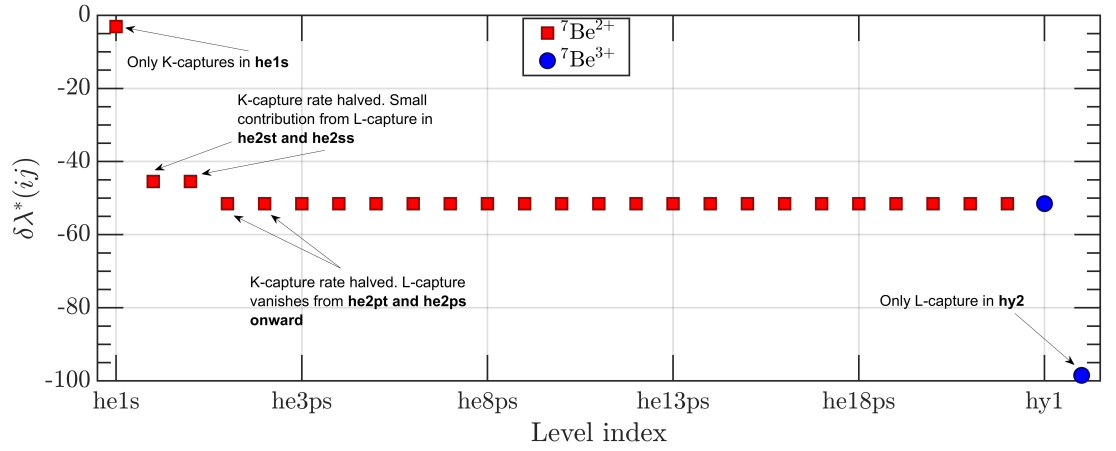


Figure 3: (a) Radial charge probability as a function of distance from the centre of the atom in ${}^7\text{Be}$ and (b) the larger of $f(x)^2$ or $g(x)^2$ at the surface of ${}^7\text{Be}$ nucleus for various orbitals. The brown, vertical, dashed line indicates the phenomenological radius of the nucleus. The $2p_{3/2}$ orbital curve falls too rapidly to be shown here.



(a)



(b)

Figure 4: Percentage change in decay rate with respect to neutral, ground state ${}^7\text{Be}$ as a function of configuration (ij) for (a) $i = 0^+, 1^+$ and (b) $i = 2^+, 3^+$. As in Fig. 2, only a few levels per ionisation stage are shown for brevity, but important levels are marked.

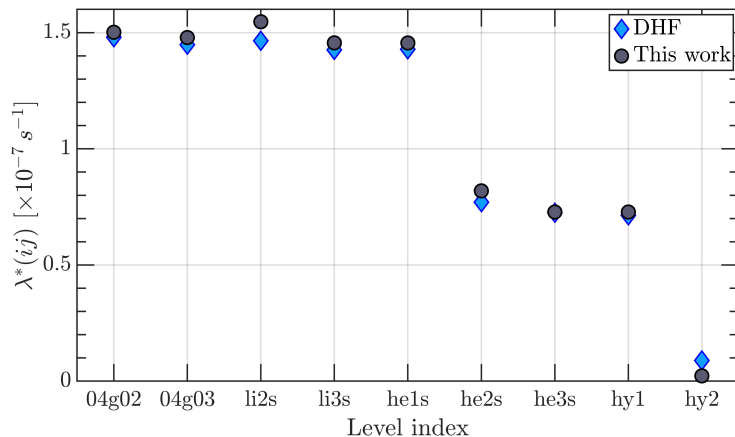


Figure 5: ${}^7\text{Be}$ configuration-dependent $\lambda^*(ij)$ calculated using our model and DHF [31, 41, 57].

due to the same overestimated capture rate predicted by our model as explained above, but the difference is quite small. When applied to neutral ${}^7\text{Be}$ in ground state (denoted by level index 04g02), the model predicts $t_{1/2} = 53.44$ days and branching ratio 10.45% which are which is well within the error limits reported in the ENSDF database [53] ($t_{1/2} = 53.22 \pm 6$ d and BR=10.44%). It should be mentioned that the $\log ft$ values had to be slightly altered to get this degree of match - $\log f_0 t = 3.371$ and $\log f_1 t = 3.650$ were used - but the differences are only 1.4% and 2.6% respectively with respect to ENSDF data, and are well within the accepted uncertainty on these parameters.

In-Plasma EC Decay Rate of ${}^7\text{Be}$

The configuration-dependent decay rates $\lambda^*(ij)$ can be converted into the in-plasma decay rates through the equation

$$\lambda^* = \sum_{ij} p_{ij} \lambda^*(ij) \quad (17)$$

where p_{ij} indicates the probability of finding the ion in the (ij) -configuration. The purpose of the plasma component of our model is to customise the formalism to evaluate p_{ij} according to the geometry and nature of the plasma.

For *uniform* plasmas (homogeneous and isotropic), we use FLYCHK to obtain p_{ij} in a large range of n_e and kT_e values. The calculations can be run in both LTE and NLTE modes, which allows us to explore plasma ion dynamics under a variety of situations and study their effect on λ^* .

Fig. 6 shows the mean charge $\langle Z \rangle$ of ${}^7\text{Be}$ as a function of kT_e for two different densities - $n_e = 10^{12} \text{ cm}^{-3}$ and $n_e = 10^{25} \text{ cm}^{-3}$ - under both LTE and NLTE conditions. The lower n_e is on the same order of magnitude as laboratory magnetoplasmas such as PANDORA, whereas the higher n_e describes

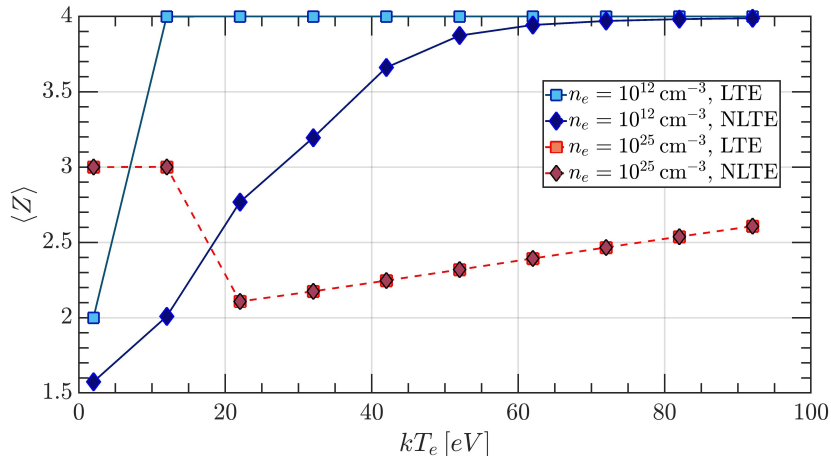
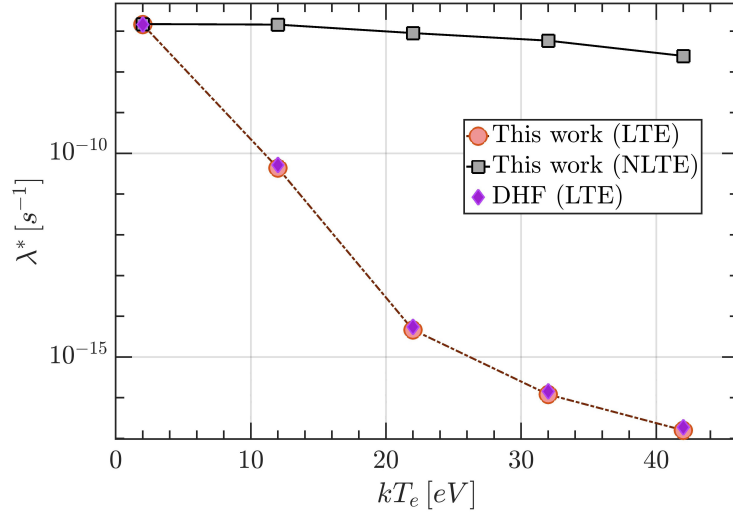


Figure 6: $\langle Z \rangle$ of ${}^7\text{Be}$ as a function of kT_e for $n_e = 10^{12} \text{ cm}^{-3}$ (blue curves) and $n_e = 10^{25} \text{ cm}^{-3}$ (red curves), in LTE (squares) and NLTE (diamonds) plasmas.

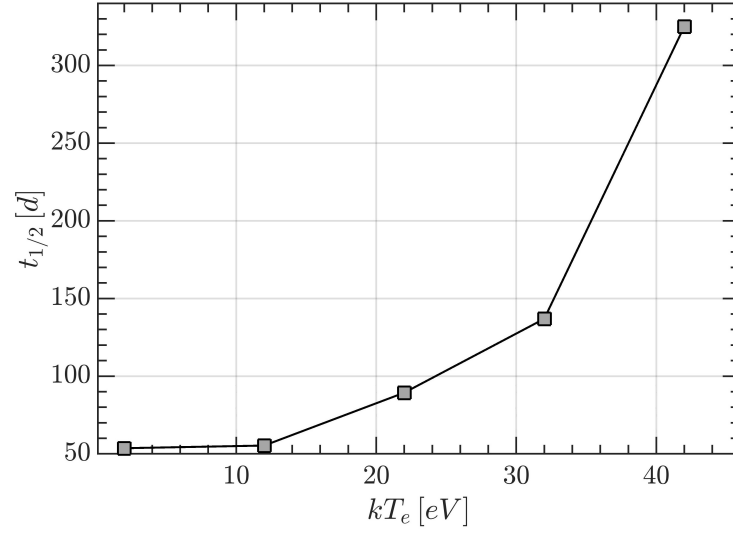
stellar interiors. It can be noticed that at low densities, LTE and NLTE plasmas show strong differences in behaviour which vary according to the plasma temperature. At low kT_e , the predicted $\langle Z \rangle$ are close, and they converge again at high kT_e . This convergence can be attributed to increased inter-level reaction rates, signalling the onset of equilibrium. At low densities, NLTE predictions can be believed to be more reliable because the plasma is not collisional enough to establish an equilibrium. High collisionality and reaction rates are present in high n_e plasmas at all temperatures, which explains the perfectly superposed LTE and NLTE $\langle Z \rangle$ curves at $n_e = 10^{25} \text{ cm}^{-3}$. These trends highlight the fact LTE-based models like TY83 cannot be directly validated in low density magnetoplasmas and therefore justifies the need to generalise the same to NLTE systems.

We use the p_{ij} predicted by FLYCHK for $n_e = 10^{12} \text{ cm}^{-3}$ and a set of $kT_e \in [2, 12, 22, 32, 42] \text{ eV}$ to calculate λ^* according to Eq. 17. Fig. 7(a) shows the in-plasma orbital EC decay rate of ${}^7\text{Be}$ as a function of kT_e , in LTE and NLTE conditions. The effect of $\langle Z \rangle$ on λ^* is clear - at $kT_e = 2 \text{ eV}$, our model predicts the same λ^* for LTE and NLTE which have similar $\langle Z \rangle$ (Fig. 6). The deviation between LTE and NLTE $\langle Z \rangle$ on increasing $kT_e \rightarrow 42 \text{ eV}$ spills over into λ^* which decreases by orders of magnitude under LTE conditions, but shows a much lower suppression in NLTE plasmas. The decay rates can be expected to converge again at $kT_e > 60 \text{ eV}$, according to the trends in Fig. 6. Our results are also benchmarked by comparing our LTE results against independent DHF calculations [31, 41, 57], which are in solid agreement. The first principle simulations of the LTE plasma using the DHF approach were performed with the in-house relativistic code DIRECT [59].

Fig. 7(b) shows the variation of $t_{1/2}$ of ${}^7\text{Be}$ in the NLTE plasma for low density $n_e = 10^{12} \text{ cm}^{-3}$. It can be observed that $t_{1/2}$ increases with kT_e because



(a)



(b)

Figure 7: (a) λ^* vs kT_e for LTE and NLTE systems, compared with DHF results (for LTE alone) and (b) variation in EC $t_{1/2}$ vs kT_e in NLTE plasma. The plasma density is fixed to $n_e = 10^{12} \text{ cm}^{-3}$.

hotter plasmas generate more 2^+ and 3^+ ions which strongly suppress capture rates (as seen in Figs. 4 and 5). At $kT_e = 42$ eV, there is already a five-fold increase in $t_{1/2}$, and it may be expected to rise even more till all ions are pushed into the $i = 4^+$ state. At this point, orbital captures will stop completely and only continuum captures will contribute to the decay of ${}^7\text{Be}$. The precise balance between orbital and continuum captures depends strongly on the density and temperature of the plasma, and has been a topic of intense study over the past few years [33, 35, 38, 41]. Preliminary DHF calculations indicate that for $n_e \sim 10^{12-13} \text{ cm}^{-3}$, continuum captures in ${}^7\text{Be}$ will be suppressed on account of low electron density at the nuclear surface, and thus the radioisotope may become completely stable. This will have a strong bearing on the planned experiments with ${}^7\text{Be}$ in PANDORA, and may have some influence on primordial nucleosynthesis models as well. The configuration-dependent EC decay rate of ${}^7\text{Be}$ as predicted by our model can also provide theory support to the experimental results obtained so far at the ERNA facility [60], and upcoming measurements.

Discussion

To investigate the validity of our model in more detail, we analyse some aspects of the atomic and plasma components separately. Fig. 8 shows the CSD p_i of ${}^7\text{Be}$ under solar conditions, as predicted by FLYCHK. The plasma parameters are taken as $n_e \sim 3.8 \times 10^{25} \text{ cm}^{-3}$ and $kT_e \sim 1.38$ keV, corresponding to mass density $\rho = 150 \text{ g/cm}^{-3}$ and temperature $T = 16 \times 10^6$ K [41]. The temperature is the same for both electrons and ions because p_i is calculated under LTE conditions which are identical to NLTE at high n_e (Fig. 6). It can be observed that $\sim 20\%$ of ${}^7\text{Be}$ is expected to be in $i = 3^+$, which means that in the sun, there is a small but non-zero contribution of orbital EC to the total decay rate. This is precisely in line with the established literature on the subject [37] per the predictions by Iben, Bahcall, Moeller and Grunzinov [33, 34, 35], and reaffirmed by Simonucci and Taioli [41]. While our model still needs to be updated to calculate the *total* capture rate on ${}^7\text{Be}$ in the sun through the addition of continuum capture and inclusion of screening effects on the electron wavefunctions, the results of Fig. 8 reinforce the validity of the plasma component of our model because they reproduce the presence of bound electrons in the plasma.

In addition, the plasma module also reproduces the expected physics of EC decay in ${}^7\text{Be}$ - as can be seen in Fig. 7(b), $t_{1/2} \rightarrow 53.2$ [d] as $kT_e \rightarrow 0$ meaning that the model inevitably reproduces the terrestrial decay rate of ${}^7\text{Be}$ when the plasma disappears.

The atomic component of the model has been validated against EC and BSBD rates of certain radio-isotopes in select (ij) configurations. As already noted before, the $t_{1/2}$ of neutral ${}^7\text{Be}$ in ground state matches the ENSDF data perfectly well. In addition, we also analyse the situation for ${}^{163}\text{Dy}$ and ${}^{140}\text{Pr}$ whose configuration-dependent decays have been experimentally studied in storage rings.

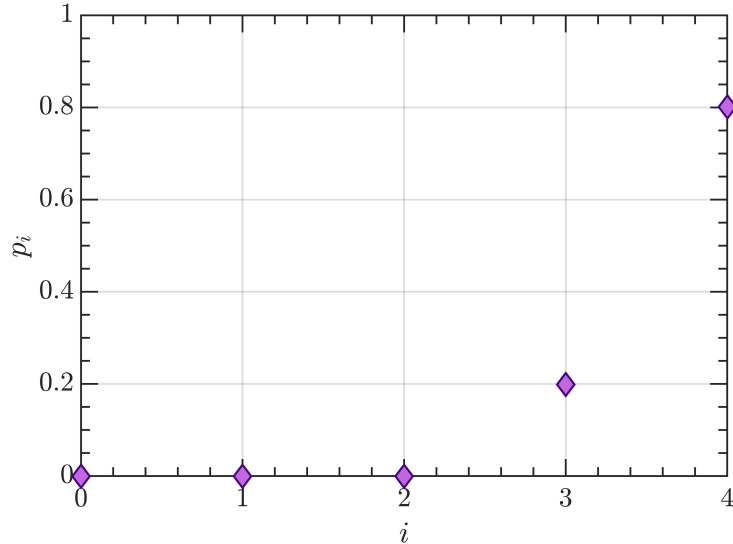


Figure 8: p_i of ${}^7\text{Be}$ for $n_e \sim 3.8 \times 10^{25} \text{ cm}^{-3}$ and $kT_e = 1.38 \text{ keV}$, corresponding to solar conditions.

${}^{163}\text{Dy}$ is stable under neutral conditions, but when fully-ionised, it undergoes BSBD with a measured $t_{1/2} = 47_{-4}^{+5} \text{ d}$ [22]. On applying Eq. 3 to ${}^{166}\text{Dy}^{66+}$ and using a single transition marked by $\log ft = 4.99$, we calculate $t_{1/2} = 49.77 \text{ d}$, which is not only within the experimental error limits, but also the same as calculated in Chang and coworkers [29] ($t_{1/2} = 49.52 \text{ d}$).

On the other hand, ${}^{140}\text{Pr}$ is an unstable element which undergoes decays through EC and β^+ , with an accepted $t_{1/2} = 3.39 \pm 1 \text{ min}$ under neutral conditions [61]. Experiments in storage rings have measured $\lambda^*(ij)$ of ${}^{140}\text{Pr}$ in fully-ionised, one-electron attached (hydrogen-like) and two-electron attached (helium-like) configurations [62]. We calculate the EC decay rate for helium-like ${}^{140}\text{Pr}^{57+}$ and obtain $\lambda^* = 0.00145 \text{ s}^{-1}$, in perfect agreement with measured rate $0.00147 \pm 7 \text{ s}^{-1}$. The authors in Ref. [62] also note that β^+ decay rates are fairly invariant over different atomic configurations, and on adding their measured $\lambda_{\beta^+}^*$ to our calculated λ_{EC}^* for neutral ${}^{140}\text{Pr}$, we obtain $t_{1/2} = 3.61 \text{ min}$ which also in full agreement with the aforementioned half-life of ${}^{140}\text{Pr}^{0+}$. A list of all isotopes analysed and results obtained is presented in Table 1. It should be noted that $t_{1/2}$ reported for ${}^{140}\text{Pr}^{57+}$ corresponds to EC decays alone, which explains the factor two difference compared to the neutral case.

In summary, we have developed a general model of in-plasma β decay which can be identically applied to a vast range of plasma parameter space. The strength of the model lies in its separation of atomic and plasma components, which allows generating more observables to validate the model against, while also maintaining versatility when dealing with diverse environments. The model

Table 1: Comparison between $t_{1/2}$ and branching ratio (BR) of some isotopes as measured in storage rings or known from literature, calculated independently by other groups, and calculated by our model

Isotope	Measured	Other works	This work
${}^7\text{Be}^{0+}$	53.22 ± 6 d [53] BR=10.44%	54.19 d (DHF [31, 57])	53.44 d BR=10.45%
${}^{163}\text{Dy}^{66+}$	47^{+5}_{-4} d [22]	49.52 d (Chang <i>et al</i> [29])	49.77 d
${}^{140}\text{Pr}^{0+}$	3.39 ± 1 min [61]		3.61 min
${}^{140}\text{Pr}^{57+}$	7.86 ± 0.4 min [62] (Only EC)		7.97 min (Only EC)

has tested well with ${}^7\text{Be}$, ${}^{163}\text{Dy}$ and ${}^{140}\text{Pr}$, and will be applied to many more radio-isotopes soon.

Currently, we are introducing several upgrades to our model to improve its applicability. First and foremost is extending the formalism to predict in-plasma continuum captures and continuum $\beta^{+/-}$ decays, complementary to the work by Gupta and coworkers [28, 30]. This extension also involves including excited nuclear states in the parent and daughter atoms and assessing their impact on the modification of $t_{1/2}$. Since these additional nuclear couplings lack literature data on their comparative half-lives, we are looking into shell model and *ab-initio* calculations to obtain better precision on $\log ft$ values, in line with the suggestions by Chang and coworkers [29].

We are also working on incorporating the effect of ionisation potential depression (IPD) on level energies which will modify $Q_m(ij)$ as a function of n_e and kT_e . With regards to EC decays, Litvinov and coworkers [62] have already identified the presence of the hyperfine splitting effect in hydrogen-like ${}^{140}\text{Pr}^{58+}$ which potentially enhances the capture rate [56]. We are working on probing the effect of the same on EC capture decay rates in ${}^{140}\text{Pr}^{58+}$ and ${}^7\text{Be}^{3+}$. And finally, to fulfill the objective of benchmarking TY83 in laboratory magnetoplasmas, we intend to couple our model with a Particle-in-Cell Monte Carlo (PIC-MC) code to simulate p_{ij} in an electron cyclotron resonance (ECR) plasma trap so as to predict 3D, space-resolved in-plasma decay rates for experimental verification by PANDORA.

References

- [1] Burbidge E.M., Burbidge G.R., Fowler W.A. and Hoyle F., Synthesis of Elements in Stars. *Reviews of Modern Physics* **29**, 4 (1957)
- [2] Cameron A.G.W, Nuclear Reactions in Stars and Nucleogenesis. *Publications of the Astronomical Society of the Pacific* **69**, 408 (1957)
- [3] Lugaro M., Pignatari M., Reifarth R. & Wiescher M., The *s*-Process and Beyond. *Annual Review of Nuclear and Particle Science* **73** (2023)

- [4] Arcones A. & Thielemann F., Origin of the Elements. *Astronomy and Astrophysics Review* **31**, 1 (2022)
- [5] Palmerini S., Busso M., Vescovi D., Naselli E., Pidatella A., Mucciola R., Cristallo S., Mascali D., Mengoni A., Simonucci S. & Taioli S., Presolar grain isotopic ratios as constraints to nuclear and stellar parameters of asymptotic giant branch star nucleosynthesis. *The Astrophysical Journal* **921** (2021)
- [6] Busso M.M., Kratz K.-L., Palmerini S., Akram W., and Antonuccio-Delogu V., Production of solar abundances for nuclei beyond Sr: The s- and r-process perspectives. *Frontiers in Astronomy and Space Science* **9** (2022)
- [7] Lisowski P.W., Bowman C.D., Russell G.J., and WenderS.A., The Los Alamos National Laboratory Spallation Neutron Sources. *Nuclear Science and Engineering* **106**, 2 (1990)
- [8] Abbondanno U. *et al*, CERN n_TOF facility: Performance report (2003)
- [9] Guerrero C. *et al*, Performance of the neutron time-of-flight facility n_TOF at CERN. *The European Physical Journal A* **49**, 1 (2013)
- [10] Emery G.T., Perturbation of Nuclear Decay Rates, *Annual Review of Nuclear Sciences* **22**, 165 (1972)
- [11] Rutherford E. & Petavel J.E., The Effect of High Temperature on the Activity of the Products of Radium, *The Collected Papers of Lord Rutherford of Nelson* **2**, pp. 456-457 (1907)
- [12] Curie M.P. & Kammerlingh-Onnes M., The radiation of radium at the temperature of liquid hydrogen, *KNAW Proceedings* **15 II**, pp. 1430-1441 (1913)
- [13] Bouchez R., Daudel P., Daudel R., Muxart R. & Rogozinski A., Mise en évidence de l'influence du degré de l'ionisation de l'atome sur la période du nuclide ${}^7\text{Be}$. *J. Phys. Radium* **10**, 201 (1949)
- [14] Leininger R.F., Segre E. & Wiegand C., Experiments on the effect of atomic electrons on the decay constant of ${}^7\text{Be}$. *Physical Review* **76**, 897 (1949)
- [15] Ray A., Das P., Sahu S., Das S., Sethi B., Mookerjee A., Chaudhuri C.B. & Pari G., Observation of large change of ${}^7\text{Be}$ decay rate in Au and Al_2O_3 and its implications. *Physical Letters B* **455**, 69 (1999)
- [16] Norman E., Rech G., Browne E., Larimer R.-M., Dragowsky M.R., Chan Y.D., Isaac M.C.P., McDonald R.J. & Smith A., Influence of physical and chemical environments on the decay rates of ${}^7\text{Be}$ and ${}^{40}\text{K}$. *Physical Letters B* **519**, 15 (2001)
- [17] Ohtsuki T., Ohno K., Morisato T., Mitsugashira T., Hirose K., Yuki H. & Kasagi J., Radioactive Decay Speedup at T=5 K: Electron-Capture Decay Rate of ${}^7\text{Be}$ Encapsulated in C_{60} . *Physical Review Letters* **98**, 1 (2007)

- [18] R. Daudel, Alteration of radioactive periods of the elements with the aid of chemical methods. *Rev. Sci.* **85** (1947)
- [19] E. Segre, Possibility of altering the decay rate of a radioactive substance. *Physical Review* **71** (1947)
- [20] Bainbridge K.T., Goldhaber M. & Wilson E., Influence of the chemical state on the lifetime of a nuclear isomer, Tc^{99m} . *Physical Review* **90**, 430 (1953)
- [21] Cooper J.A., Hollander J.M. & Rasmussen J.O., Effect of the chemical state on the lifetime of the 24-second isomer of Nb^{90*} . *Physical Review Letters* **15**, 680 (1965)
- [22] Jung M. *et al*, First Observation of Bound-State β -Decay. *Physical Review Letters* **69**, 2164 (1992)
- [23] F. Bosch *et al*, Observation of Bound-State β -Decay of Fully Ionized ^{187}Re : ^{187}Re - ^{187}Os Cosmochronometry. *Physical Review Letters* **77**, 5190 (1996)
- [24] Litvinov Y. and Chen R.J., Radioactive decays of stored highly charged ions. *The European Physical Journal A* **59**, 102 (2023)
- [25] Daudel R., Jean M. & Lecoïn M., On the possible existence of a particular type of e^- creating radioactive phenomenon. *J. Phys. Radium* **8**, 238 (1947)
- [26] Morisato T., Ohno K., Ohtsuki T., Hirose K., Sluiter M. & Kawazoe Y., Electron-capture decay rate of $^7\text{BeC}_{60}$ by first-principles calculations based on density functional theory. *Physical Review B* **78**, 1 (2008)
- [27] Lee K. & Stenle-Neumann G., Ab-initio study of the effects of pressure and chemistry on the electron-capture radioactive decay constants of ^7Be , ^{22}Na and ^{40}K , *Earth and Planetary Science Letters* **267**, 628 (2008)
- [28] Gupta A., Lahiri C., and Sarkar S., Bound and continuum state β -decay of bare atoms: Enhancement of decay rate and changes in β -decay branching, *Physical Review C* **100**, 1 (2019)
- [29] Liu S., Gao C., and Xu C., Investigation of bound state β -decay half-lives of bare atoms. *Physical Review C* **104**, 1 (2021)
- [30] Gupta A., Lahiri C., and Sarkar S., Allowed β^- decay of bare atoms with $A \approx 60 - 80$ in stellar environments, *Physical Review C* **108**, 015805 (2023)
- [31] Taioli S., Vescovi D., Busso M., Palmerini S., Cristallo S., Mengoni A. & Simonucci S., Theoretical Estimate of the Half-Life for the Radioactive ^{134}Cs and ^{135}Cs in Astrophysical Scenarios, *The Astrophysical Journal* **933**, 148 (2022)
- [32] J. Bahcall, Electron Capture and Nuclear Matrix Elements of Be^7 . *Physical Review* **128**, 1297 (1962)

- [33] Iben Jr I., Kalata K. & Schwartz J., The effect of Be^7 K-Capture on the solar neutrino flux. *The Astrophysical Journal* **150**, 1001 (1967)
- [34] Bahcall J. & C. Moeller, The ^7Be Electron-Capture rate. *The Astrophysical Journal* **155**, 511 (1969)
- [35] Gruzinov A.V. & Bahcall J., The ^7Be electron capture rate in the sun. *The Astrophysical Journal* **490**, 437 (1997)
- [36] Johnson, C.W., Kolbe, E., Koonin S.E. & Langanke K., The Fate of ^7Be in the Sun. *Astrophysical Journal* **392** (1992)
- [37] Adelberger E.G. *et al*, Solar fusion cross sections. II. The pp chains and CNO cycles. *Review of Modern Physics* **83**, 1 (2011)
- [38] Shaviv N. & Shaviv G., The state of ^7Be in the core of the Sun and the solar neutrino flux. *Monthly Notices of the Royal Astronomical Society* **341**, 119 (2003)
- [39] Quarati P. & Scarafone A., Nuclear electron capture rate in stellar interiors and the case of ^7Be . *Journal of Physics G: Nuclear and Particle Physics* **36**, 1 (2008)
- [40] Sawyer R., Electron capture rates in a plasma. *Physical Review C* **83**, 1 (2011)
- [41] Simonucci S., Taioli S. Palmerini S. & Busso M., Theoretical estimates of stellar e^- captures. I. The half life of ^7Be in evolved stars. *The Astrophysical Journal* **764**, 1 (2013)
- [42] Vescovi D., Piersanti L., Cristallo S., Busso M., Vissani F., Palmerini S., Simonucci S. & Taioli S., Effects of a revised ^7Be e^- -capture rate on solar neutrino fluxes. *Astronomy and Astrophysics* **623**, A126 (2019)
- [43] Broggini C., Canton L., Fiorentini G. & Villante F.L., The cosmological ^7Li problem from a nuclear physics perspective. *Journal of Cosmology and Astroparticle Physics* **2012** (2012)
- [44] Bahcall J., Theory of Bound-State Beta Decay. *Physical Review* **124**, 495 (1961)
- [45] Bahcall J., Beta Decay in Stellar Interiors. *Physical Review* **126**, 1143 (1962)
- [46] Bahcall J., Electron Capture in Stellar Interiors. *The Astrophysical Journal* **139**, 318 (1964)
- [47] Takahashi K. and Yokoi K., Nuclear β -Decays of Highly Ionised Heavy Atoms in Stellar Interiors. *Nucl. Phys. A* **404**, 578 (1983)

- [48] Mascali D., Musumarra A., Leone F. Romano F.P., Galatá A., Gammino S. and Massimi C., PANDORA, a new facility for interdisciplinary in-plasma physics. *The European Physical Journal A* **53**, 145 (2017)
- [49] Leach K.G., Dillmann I., Klawitter R., Leistenschneider E., Lennars A., Brunner T., Frekkers D., and Andreiou C., Electroweak Decay Studies of Highly Charged Radioactive Ions with TITAN at TRIUMF. *Atoms* **5**, 1 (2017)
- [50] Musumarra A., Massimi C., Pellegriti M.G., and Leone F., Ion Traps for Nuclear Decay Studies: a design for a handheld Electron Beam Ion Trap (EBIT). *HNPS Advances in Nuclear Physics* **29**, (2023)
- [51] Mascali D., Santonocito D. *et al*, A Novel Approach to β -Decay: PANDORA, a New Experimental Setup for Future In-Plasma Measurements. *Universe* **8**, 1 (2022)
- [52] Chung H.-K., Chen M., Morgan W., Ralchenko Y. & Lee R., FLYCHK: Generalized population kinetics and spectral model for rapid spectroscopic analysis for all elements. *High Energy Density Phys.* **1**, 3 (2005)
- [53] Tilley D., Cheves C., Godwin J., Hale G., Hofmann H., Kelley J., Sheu C. & Weller H., Energy levels of light nuclei $A = 5, 6, 7$. *Nuclear Physics A* **708**, 3 (2002)
- [54] Lee R.W. and Larsen J.T., A time-dependent model for plasma spectroscopy of K-shell emitters, *Journal of Quantitative Spectroscopy and Radiative Transfer* **56**, 4 (1996)
- [55] Bar-Shalom A. and Oreg, J., HULLAC, an integrated computer package for atomic processes in plasmas, *Journal of Quantitative Spectroscopy and Radiative Transfer* **71**, 2-6 (2001)
- [56] Folan L. & Tsifrinovich V., Effects of the Hyperfine Interaction on Orbital Electron Capture. *Physical Review Letters* **74**, 499 (1995)
- [57] Morresi T., Taioli S. & Simonucci S., Relativistic Theory and Ab Initio Simulations of Electroweak Decay Spectra in Medium-Heavy Nuclei and of Atomic and Molecular Electronic Structure. *Advanced Theory and Simulations: Nuclear Beta Decay* **1**, 11 (2018).
- [58] Burke V. & Grant I., The effect of relativity on atomic wave functions. *Proceedings of the Physical Society* **90**, 297 (1967).
- [59] Taioli S. & Simonucci S., Relativistic quantum theory and algorithms: a toolbox for many-fermion systems in different scenarios. *Annual Reports in Computational Chemistry* **17** (2021)
- [60] Santonostaso C., Buompane R., Di Leva A., Morales-Gallegos L., Itaco N., Landi G., Leitzert H.C., Rapagnani D. & Gialanella L., Change in the ${}^7\text{Be}$ half-life in different environments. *Il Nuovo Cimento* **44 C**, 75 (2021)

- [61] Nica N., Nuclear Data Sheets for A=140, *Nuclear Data Sheets* **154** (2018).
- [62] Litvinov Y., Measurement of the β^+ and Orbital Electron-Capture Decay Rates in Fully Ionized, Hydrogenlike, and Heliumlike ^{140}Pr Ions, *Physical Review Letters* **99** 262501 (2007).

Acknowledgements

The authors gratefully acknowledge the support of 3rd National Committee of INFN and funding from project PANDORA.Gr3. A.P. would like to acknowledge the financial support from the MUR-PNRR Project PE0000023-NQSTI, financed by the European Union (NextGeneration EU). S.T. would like to acknowledge the European Union under grant agreement no. 101046651 for this action. The authors are grateful to Chang Xu and Shuo Liu at the School of Physics, Nanjing University, China, for clarifying the meaning of the equations used to calculate the radial wavefunctions on the nuclear surface.

Appendix - FLYCHK Data

Data on the excitation levels in ions, their energy and electronic configurations used in this model is taken from the atomic physics database employed by FLYCHK. FLYCHK is a population kinetics code which can calculate CSD and LPD of ions for different kinds of plasma in various configurations [52]. The code is a successor to the FLY suite of codes [54] and is capable of generating detailed spectra of plasma in a broad wavelength range. In order to do so, FLYCHK uses an extensive repository of atomic data for elements from $Z = 1 - 71$ which includes valuable info like level electronic configuration, energy, oscillation strength and statistical weight.

The nomenclature of atomic levels in FLYCHK is a combination of existing names from the FLY module [54], the HULLAC database [55] and superconfiguration states. A detailed explanation of each is provided in Ref. [52] but a brief summary is provided here. When performing computations for H-, He- and Li-like ions (meaning one, two and three electrons attached, respectively), FLYCHK uses the FLY database for $Z \leq 26$, and the HULLAC database for others. Consequently, levels in $^7\text{Be}^{1/2/3+}$ and $^7\text{Li}^{0/1/2+}$ follow the FLY nomenclature while those in neutral $^7\text{Be}^{0+}$ follow FLYCHK's own system of nomenclature instead. The atomic levels are broadly categorised as bound and autoionising, depending on their energy - the former are levels with energy less than the ionisation energy of the atom/ion whereas the latter are free states that automatically collapse into the next ionisation state. The plasma decay model described in this work only considers bound levels.

As may be seen from Figs.1 and 2(a), levels in $^7\text{Be}^{0+}$ are named as $04g[n]$ where $[n]$ ranges from 02–10. The first index 04 represents 4 electrons present in the system, while g represents bound states. $[n]$ denotes the principal quantum number of the valence electron but no detailed information on the subshell

Table 2: FLYCHK level notations and description

Level	Spectroscopic Notation	Shell Description
04g02	$(1s)^2(2s2p)^2$	Averaged over l (K^2L^2)
04g03	$(1s)^2(2s2p)^1(3s3p3d)^1$	Averaged over l ($K^2L^1M^1$)
04g07	$(1s)^2(2s2p)^1(7s7p7d7f7g7h7i)^1$	Averaged over l ($K^2L^1Q^1$)
li2s	$(1s)^2(2s)^1$	Averaged over m_l (K^2L^1)
li3p	$(1s)^2(3p)^1$	Averaged over m_l (K^2M^1)
li7	$(1s)^2(7s7p7d7f7g7h7i)^1$	Averaged over l (K^2Q^1)
he1s	$(1s)^2$	Ground state (K^2)
he2st	$(1s)^1(2s)^1\ ^3S$	Spin triplet (K^1L^1)
he2ss	$(1s)^1(2s)^1\ ^1S$	Spin singlet (K^1L^1)
he2ps	$(1s)^1(2p)^1\ ^3S$	Spin triplet, averaged over m_l (K^1L^1)
he7ps	$(1s)^1(10p)^1\ ^1S$	Spin singlet, averaged over m_l (K^1Q^1)
hy1	$(1s)^1$	Ground state (K^1)
hy3	$(3s3p3d)^1$	Averaged over l (M^1)

configuration is available. This is the reason behind the imprecise estimation of σ_{2s} in EC rates in neutral ${}^7\text{Be}$, which leads to a relative overestimation in the same at li2s.

Levels in ${}^7\text{Be}^{1+}$ and ${}^7\text{Li}^{0+}$ are generally designated as li[nl] where [nl] represents the principal and azimuthal quantum numbers respectively. This detailed notation lasts till $n = 5$, after which only n is shown. This implies that subshell configuration details from li6 onward do not exist.

In case of ${}^7\text{Be}^{2+}$ and ${}^7\text{Li}^{1+}$, the level notations follow the general structure he[nls] where [nls] stands for principal and azimuthal quantum numbers of the valence electron, and total spin state respectively. This level of detail holds till $n = 2$ beyond which the indices collapse to the simpler form he[nps].

The levels of ${}^7\text{Be}^{3+}$ and ${}^7\text{Li}^{2+}$ are simply represented as the hydrogenic hy[n] where n is the principal quantum number of the one attached electron. A short summary of the level indices and their characteristics is provided in Table 2.